ACS OMEGA

http://pubs.acs.org/journal/acsodf

Article

Study on the Adsorption Mechanism of Cobalt and Nickel in Manganese Sulfate by δ-MnO_2

Pan Yang,[#] Jiawei Wang,[#] Song Wang, Chunyuan Yang, Pingyuan Zhao, Bifang Huang, Qin Wang, and Haifeng Wang*

Cite This: *ACS Omega* 2022, 7, 37452−37464

Read Online

ACCESS | Metrics & More | Article Recommendations

ABSTRACT: Manganese has excellent performance in removing metal ions from aqueous solutions, but there are few studies on the adsorption and removal of heavy metal impurities in metal salt solutions. In this paper, the adsorption of cobalt and nickel ions in $MnSO_4$ solution by δ-MnO_2 prepared from two different manganese sources was studied. The optimum adsorption conditions were as follows: When the concentration of Mn^{2+} was 20 g/L, δ-MnO_2 addition was 10 g/L, Co^{2+} concentration was 80 mg/L, Ni^{2+} concentration was 80 mg/L, reaction time was 60 min, reaction temperature was 80 °C, and pH value was 7, the adsorption rate of Co^{2+} and Ni^{2+} reached more than 80%. The manganese dioxide adsorbed by heavy metals was analyzed and detected. The results showed that MnOOH appeared in the phases of both kinds of δ-MnO_2, and their morphologies were dense rod-like structures with different lengths and flake-like structures of fine particles. Co and Ni were distributed on the surface and gap of MnO_2 particles, and the atomic percentage of Co was slightly higher than that of Ni. The new vibration peaks appeared near wave numbers of 2668.32, 1401.00, and 2052.19 cm^{-1}, which were caused by the complexation of cations such as Co^{2+} and Ni^{2+} with hydroxyl groups. Some cobalt and nickel appeared on the surface of δ-MnO_2, and the surface oxygen increased after adsorption. The above characterization revealed that the adsorption of cobalt and nickel in manganese sulfate by δ-MnO_2 was realized by the reaction of its surface hydroxyl with metal ions (M) to form ≡SOMOH.

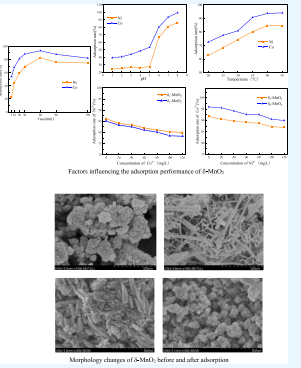

1. INTRODUCTION

Manganese sulfate is the most important and basic manganese source material for manganese-based lithium battery cathode materials.[1−5] It is also the raw material for the preparation of manganese oxides, so it is of great significance to prepare high-purity manganese sulfate.[6−9] In manganese ore, heavy metal cobalt and nickel often exist in the form of association. Therefore, when manganese ore is leached to obtain manganese sulfate, the impurity metals Co and Ni will also be leached one after another, resulting in the high content of heavy metal ions in the leached manganese sulfate solution, which seriously affects the quality of subsequent products. For example, the purity of manganese-based materials, especially the content of heavy metal impurities, is directly related to the specific capacity of the battery and the number of charge and discharge times.[3] Battery-grade manganese sulfate has strict requirements on various metal impurity ions. The key to preparing high-purity manganese sulfate is to remove impurities. To obtain high-quality manganese-based battery materials, the purity of manganese-based raw materials must first be ensured. Whether it is manganese sulfate directly used to produce ternary materials or manganese oxide used to produce lithium manganate, it is necessary to first obtain manganese sulfate with high purity. Manganese sulfate is the most important and basic manganese source material for cathode materials of manganese-based power lithium batteries. So it is necessary to remove impurities in the manganese sulfate solution to obtain high-purity manganese sulfate products.[10,11] The common impurity removal methods include the sulfide precipitation method,[12−14] fluorination method,[15−17] carbonation method,[18,19] extraction method,[20] and crystallization method.[21,22] There are many shortcomings such as the long procedure, many control nodes, high requirements, high cost, large amount of slag, and low efficiency in the above processes. Therefore, developing an effective, short process with low environmental harm, low cost, and low slag removal has become a research hotspot in manganese sulfate production.

The adsorption method has been more and more widely used because of its simple process, good economic benefit, high treatment efficiency, and environmental friendliness,[23−27] and the heavy metal ions in the adsorbent could be recycled by resolution so as to realize the regeneration and recycling of the adsorbent.[28,29] Adsorption is the phenomenon of automatic

Received: July 6, 2022
Accepted: September 12, 2022
Published: October 12, 2022

diffusion and enrichment of molecules or ions between solid−liquid interfaces. According to this principle, the target molecules or ions are removed from the solution by using adsorbents with large specific surface area and high surface energy.[30] MnO_2 is an excellent adsorbent because of its rich surface hydroxyl, many defects, large specific surface area, and strong ion exchange capacity.

Manganese dioxide is mainly used in the field of adsorption to adsorb heavy metal ions in wastewater and alleviate the pressure of heavy metal pollution on the environment.[31−37] Wang[38] studied the adsorption properties of heavy metals antimony and thallium. δ-MnO_2 had the best adsorption properties for Sb(III) and Tl(I), and its maximum adsorption capacities reached 120 and 498 $mg{\cdot}g^{-1}$, respectively. δ-MnO_2 was prepared by Kong and Zhu[39] in a laboratory method, and its adsorption properties for Zn^{2+}, Cd^{2+}, Cu^{2+}, Pb^{2+}, Ni^{2+}, and Co^{2+} in the mixed metal ion system was studied. The initial pH and adsorption time of the solution were investigated. Effect of coexisting ions and ionic strength on adsorption. The results showed that when the initial pH > 3.2, the adsorbent showed good removal effects on Zn^{2+}, Cd^{2+}, Cu^{2+}, Pb^{2+}, Ni^{2+}, and Co^{2+}. The manganese oxide prepared by Kanungo et al.[40] by the method of reducing potassium permanganate had a high adsorption capacity for heavy metal ions. Oscarson and Huang[41] studied the removal of As(III) by δ, α, β state manganese dioxide. The results showed that the removal effect was related to the degree of crystallization and surface characteristics of manganese dioxide, indicating that δ, α state manganese dioxide with high activity can alleviate the toxicity of As(III) in the natural environment. Chen and Ye[42] found that manganese dioxide had a strong adsorption effect on As(III) in the oxidation adsorption test of wastewater containing As(III) by pyrolusite, and the adsorption capacities of different forms of manganese oxides were also different. Two kinds of manganese dioxide, α-MnO_2 and δ-MnO_2, were prepared by Li.[43] By controlling the single factor conditions, the main factors affecting the adsorption of nickel by manganese oxides were analyzed and studied. When the dosage was above 10 mmol, the adsorption rate of a 100 mL nickel solution with a 2 mmol/L concentration was close to 100%.

Although manganese dioxide has a good adsorption effect on heavy metal ions in water, the adsorption of heavy metal ions in high concentration metal salt solutions has been a difficult problem in the field of adsorption, and the related research is scarce. Some researchers investigated the effect of salt concentration (potassium salt, sodium salt, etc.) on the adsorption performance of manganese dioxide in the study of heavy metal ion adsorption. It was found that the adsorption amount of heavy metals was greatly weakened when there was a small amount of salt in the solution, and the adsorption amount was seriously slowed down with the increase of salt concentration. For the anion form of heavy metal impurity ions, the interference of salt solution was weak. In the mixed solution system of 80 g/L NaCl and 15 g/L Na_2SO_4, Yao[44] studied the adsorption properties of flower-like manganese dioxide and sea-urchin-like manganese dioxide for trivalent arsenic. When the additive dosage was 30 g/L, the arsenic removal rates of the two adsorbents were 97.60 and 96.06%. The adsorption behavior of manganese dioxide on molybdenum ion in a manganese sulfate solution had been discussed by Xia et al.[45,46] and Chen et al.[47,48] Through in-depth analysis, it was found that the reason why arsenic ions and molybdenum ions can overcome the influence of high concentration salts mainly depends on the fact that both ions exist in the form of anionic groups such as H_2AsO^{3-}, $HAsO_3^{2-}$, MoO_4^-, and $HMoO_4^-$ in a certain pH range to be adsorbed by MnO_2, while a large number of metal cations in high concentration salt solutions had limited obstacles to their anionic groups, so molybdenum ions in the manganese sulfate solution could be better adsorbed by manganese dioxide. However, there was no obvious effect on the metal ions in the cation form in the manganese sulfate solution.

To solve the problem of manganese dioxide adsorption of metal ions in the manganese sulfate solution, the adsorption mechanism of manganese dioxide was further studied. There are many studies on adsorption mechanism considering the influence of surface charge. The isoelectric point and zero charge of manganese dioxide are proposed,[49] but the influence of surface defects and surface hydroxyl is less mentioned.[50] Due to more or less defects, vacancies, and impurities in MnO_2, oxygen coordination around manganese vacancies was unsaturated, resulting in the presence of a large number of hydroxyl groups. When MnO_2 adsorbed heavy metal ions by surface hydroxyl complexation, the first effect was on pH.[51] Therefore, Li Mingdong, of our research group, did the determination of different crystal MnO_2 acid point pH,[52] and he compared different crystal manganese dioxide adsorption of cobalt and nickel in manganese sulfate solution. He did the analysis of its influencing factors and explored the interaction between manganese dioxide and manganese sulfate solution.[53] On this basis, this paper explored the process conditions of manganese dioxide adsorption of metal ions in heavy metal salt solutions, analyzed the surface hydroxyl complexation mechanism, and further studied the adsorption characteristics of MnO_2 surface hydroxylation on heavy metal ions. The adsorption mechanism of impurity ions in high-salt solutions was theoretically clarified to solve the difficult removal of heavy metal ions in the manganese sulfate solution, the raw material of manganese battery. Using manganese dioxide to adsorb cobalt and nickel impurities in manganese sulfate, on the one hand, can provide a reference method for manganese sulfate impurity removal to achieve battery-level requirements; on the other hand, it can recycle the adsorbed nickel and cobalt metal impurities, which has important economic significance. In this paper, the mechanism of manganese dioxide adsorbing cobalt and nickel in the manganese sulfate solution had been studied. Adsorption conditions were explored only in a simpler manganese sulfate solution system. It is hoped that, in the future, this study can be used to adsorb cobalt and nickel in a more complex manganese sulfate solution system and provide reference for adsorbing other impurity ions in heavy metal salt solutions.

2. RESULT AND DISCUSSION

2.1. Study on the Adsorption Process. Researchers in our group had done a lot of preliminary work,[53] and through the comparison of different crystal forms of manganese dioxide, the best adsorption performance was by δ-MnO_2. δ-MnO_2 prepared with different manganese sources was further studied, and the equi-acidity point pH,[53] specific surface area, pore size, and pore volume of the isoacid point were detected. Studies had shown that when the pH of the electrolyte solution is higher than the equi-acidity point pH of MnO_2, the surface hydroxyl groups undergo deprotonation reaction and complex with metal ions to release H^+, reducing the pH value of the solution. When the pH of the solution was lower than the equi-acidity point pH, the protonation reaction of the surface hydroxyl mainly consumed H^+, which increased the pH value. When the pH of the solution

https://doi.org/10.1021/acsomega.2c04240
ACS Omega 2022, 7, 37452−37464

was the same as the equi-acidity point pH, the H^+ was released by the surface hydroxyl complexation reaction and the protonation reaction consumed H^+ in a dynamic equilibrium, and the pH value did not change. The pH value of the equi-acidity point of MnO_2 is essentially the equilibrium pH value of the adsorption and desorption of the surface hydroxyl and metal ions, and the pH value of the equi-acidity point depends on the content of the surface hydroxyl and the complexation ability. Both δ_1-MnO_2 and δ_2-MnO_2 have abundant surface hydroxyl groups, but the pH values at the equi-acidity point are quite different. δ_1-MnO_2 is much higher than δ_2-MnO_2, indicating that δ_2-MnO_2 has a stronger surface hydroxyl complexing ability, so it is speculated that it has a greater adsorption potential. It can be seen from Figure 1 that the isoelectric points of δ_1-MnO_2 and δ_2-

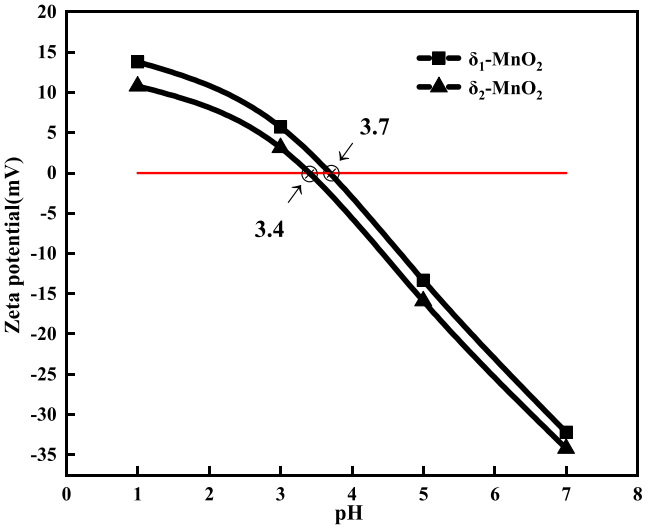

Figure 1. Surface zeta potential of δ-MnO_2.

MnO_2 are 3.7 and 3.4, respectively. When the solution pH was lower than the equi-acidity point pH, the surface of MnO_2 was positively charged. When the solution pH was higher than the equi-acidity point pH, the surface of MnO_2 was negatively charged, and the heavy metal cations in the solution could be adsorbed by charge attraction.

The two kinds of δ-MnO_2 have a pore structure, and the average pore diameter is large. The pore volume and average pore diameter of δ_2-MnO_2 are higher than those of δ_1-MnO_2. It can be seen from Figure 2 that the adsorption and desorption isotherms of the two kinds of δ-MnO_2 show the fourth type, and there is an obvious hysteresis loop. δ_1-MnO_2 belongs to the H1 hysteresis loop, which is caused by the difference in the regular shape of the pores and the size distribution of the narrow pores. The pore size distribution can be found to be mainly in the range of 2−10 nm. δ_2-MnO_2 belongs to the H3 type hysteresis loop, and the MnO_2 is composed of disc-shaped particles. The pores are slit-shaped. It can be found from the pore size distribution that most of the pores are distributed in the range of 2−10 nm, and there are still some pores in the range of 10−100 nm. The macropore structure is more abundant than δ_1-MnO_2.

From Table 1 and the above analysis, the adsorption performance of δ_2-MnO_2 should be slightly better than that of δ_1-MnO_2. It can also be found from the study of Li et al. that the adsorption efficiency of δ_2-MnO_2 on cobalt and nickel is higher than that of δ_1-MnO_2. In this paper, based on the two δ-MnO_2 adsorption conditions of Li et al.,[53] 20 g/L Mn^{2+} concentration

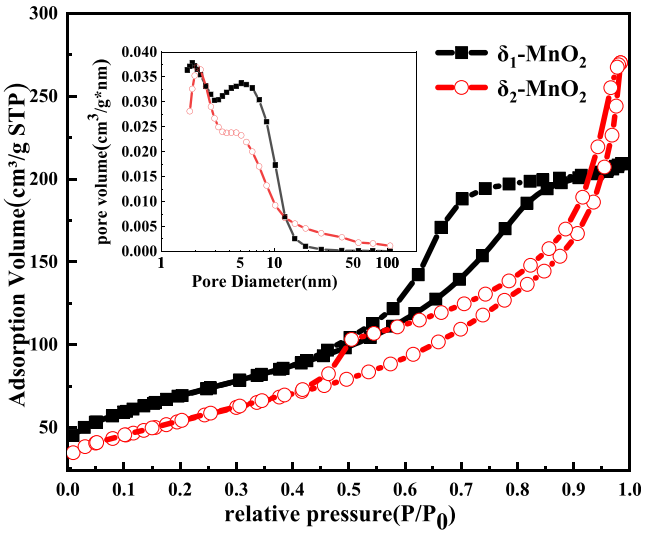

Figure 2. Nitrogen adsorption−desorption curve of δ-MnO_2.

Table 1. Partial Performance Parameters of Two Kinds of δ-MnO_2

MnO_2 crystal form	specific surface area (m^2/g)	equi-acidity points pH	isopotential point	aperture (nm)	pore volume (cm^3/g)
δ_1-MnO_2	217.42	3.85	3.7	5.2627	0.323685
δ_2-MnO_2	223.46	1.40	3.4	8.5211	0.417930

and 10 g/L MnO_2 addition were obtained as the better conditions. The optimal reaction time, reaction temperature, reaction pH, Co^{2+} concentration, and Ni^{2+} concentration were further explored; the adsorption efficiency of MnO_2 for Co^{2+} and Ni^{2+} was determined; and the influence of process conditions on the adsorption performance of MnO_2 was analyzed.

2.1.1. Effect of Reaction Time. When the Co^{2+} concentration was 80 mg/L; the Ni^{2+} concentration was 80 mg/L; the reaction temperature was 80 °C; the reaction pH was 7; and the reaction time was 5, 10, 20, 30, 60, 90, and 150 min, respectively, the adsorption rate of Co^{2+} and Ni^{2+} in manganese sulfate by δ-MnO_2 was as shown in Figure 3.

It can be seen from Figure 3 that with the increase of reaction time, the adsorption of δ-MnO_2 on Co^{2+} and Ni^{2+} first increased and then decreased. When the reaction time was 60 min, the adsorption rate reached the highest. The adsorption reaction of the two kinds of δ-MnO_2 in the first 30 min was faster due to the fact that the surface hydroxyl of δ-MnO_2 adsorption sites have not been occupied. Co^{2+} and Ni^{2+} adsorption probability is the largest, the surface complex reaction is intense, and the solution pH decreased rapidly. When the reaction time was 30−60 min, the adsorption sites were gradually occupied, the complexation reaction decreased, the pH of the solution decreased slowly, the pH adjustment times were less, and the adsorption rate of Co^{2+} and Ni^{2+} slowed down. At 60 min, the adsorption amount reached saturation. At this time, the adsorption and desorption maintained a dynamic equilibrium. The pH of the solution no longer decreased and remained stable at about 7. The adsorption amounts of Co^{2+} and Ni^{2+} reached the maximum. After 60 min, the adsorption rate decreased due to the shedding of Co^{2+} and Ni^{2+} adsorbed in MnO_2 pores and attracted by charge, and the

https://doi.org/10.1021/acsomega.2c04240
ACS Omega 2022, 7, 37452−37464

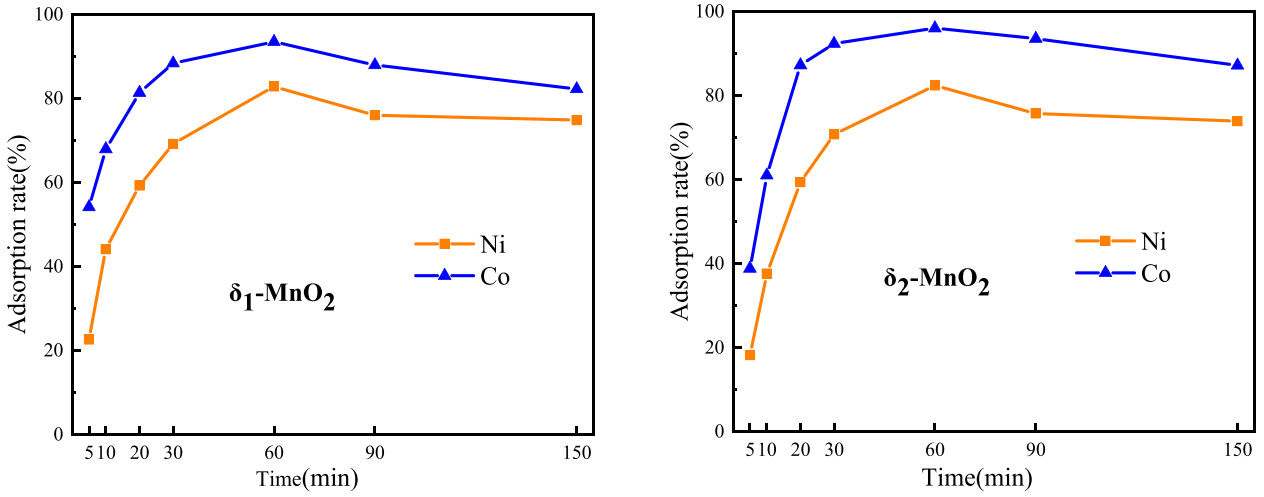

Figure 3. Effect of reaction time on the adsorption of Co^{2+} and Ni^{2+}.

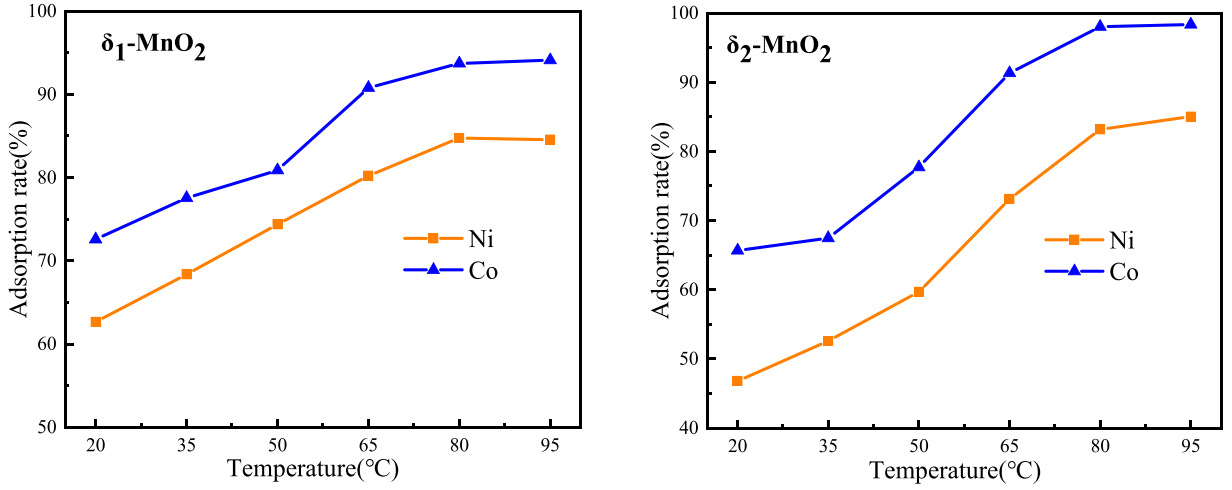

Figure 4. Effect of temperature on the adsorption of Co^{2+} and Ni^{2+}.

ion exchange reaction between other ions and adsorbed Co^{2+} and Ni^{2+}. So the appropriate reaction time was 60 min.

The adsorption rate of δ_1-MnO_2 is higher in 10 min, and that of δ_2-MnO_2 is higher in 10−60 min. The above phenomenon is due to the slit-like shape of the internal pores of δ_2-MnO_2, and the ion diffusion in the interlayer needs a longer time to diffuse to the corresponding adsorption point, so the adsorption rate is lower. After 10 min, the diffusion adsorption process is no longer a limitation of the adsorption rate.[54] More binding sites will have a higher adsorption rate. δ_2-MnO_2 has larger specific surface area, pore size, and pore volume, which can provide more adsorption sites, so the adsorption rate is higher.

2.1.2. Effect of Temperature. When the Co^{2+} concentration was 80 mg/L; the Ni^{2+} concentration was 80 mg/L; the reaction time was 60 min; the reaction pH was controlled at 7; and the reaction temperature was 20, 35, 50, 65, 80, and 95 °C, respectively, the adsorption rate of Co^{2+} and Ni^{2+} in manganese sulfate by δ-MnO_2 was as shown in Figure 4.

It can be seen from Figure4 that the adsorption rate of δ-MnO_2 for Co^{2+} and Ni^{2+} increased with the increase of reaction temperature. Since the adsorption of δ-MnO_2 was mainly due to the complexation reaction of surface hydroxyl, the higher the reaction temperature was, the more intense the movement of Co^{2+} and Ni^{2+} in the solution was, the higher the possibility of binding with hydroxyl was, and the faster the reaction was. When the temperature reached 80 °C, the adsorption rate was basically unchanged, the adsorption amount and desorption amount were in a dynamic equilibrium, and the adsorption of manganese dioxide reached saturation. It was of little significance to continue to increase the temperature. When the temperature was lower than 65 °C, the adsorption rate of δ1-MnO_2 for the two ions was higher. When the temperature was higher than 65 °C, the adsorption rate of δ_2-MnO_2 for the two ions was higher, and δ_2-MnO_2 was more affected by temperature, indicating that, at lower temperatures, the slit pore structure of δ_2-MnO_2 limited the binding of Co^{2+} and Ni^{2+} with internal adsorption sites, and the adsorption rate of δ_1-MnO_2 with a regular pore structure was higher. At higher temperatures, Co^{2+} and Ni^{2+} were more active, and the adsorption rate of δ_2-MnO_2 with a larger pore volume was higher. Therefore, the increase of temperature is beneficial to the reaction, and the adsorption reaction belongs to the endothermic reaction, which is mainly affected by the surface hydroxyl complexation. There are differences in the adsorption rate of two kinds of δ-MnO_2 with different pore structures and sizes.

2.1.3. Effect of pH Value. When Co^{2+} concentration was 80 mg/L; Ni^{2+} concentration was 80 mg/L; reaction time was 60 min; reaction temperature was 80 °C; and reaction pH value was

https://doi.org/10.1021/acsomega.2c04240
ACS Omega 2022, 7, 37452−37464

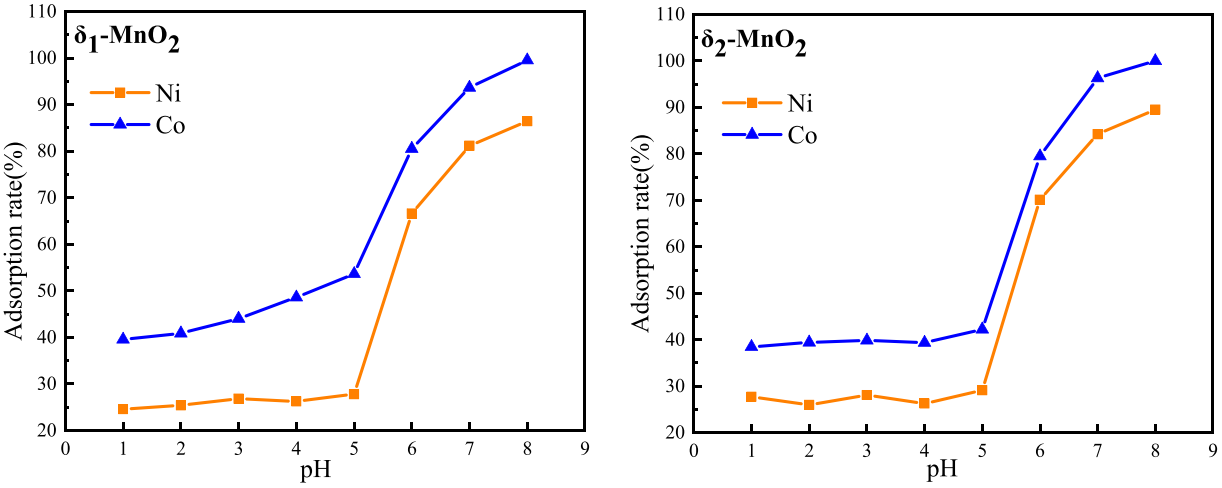

Figure 5. Effect of pH value on the adsorption of Co^{2+} and Ni^{2+}.

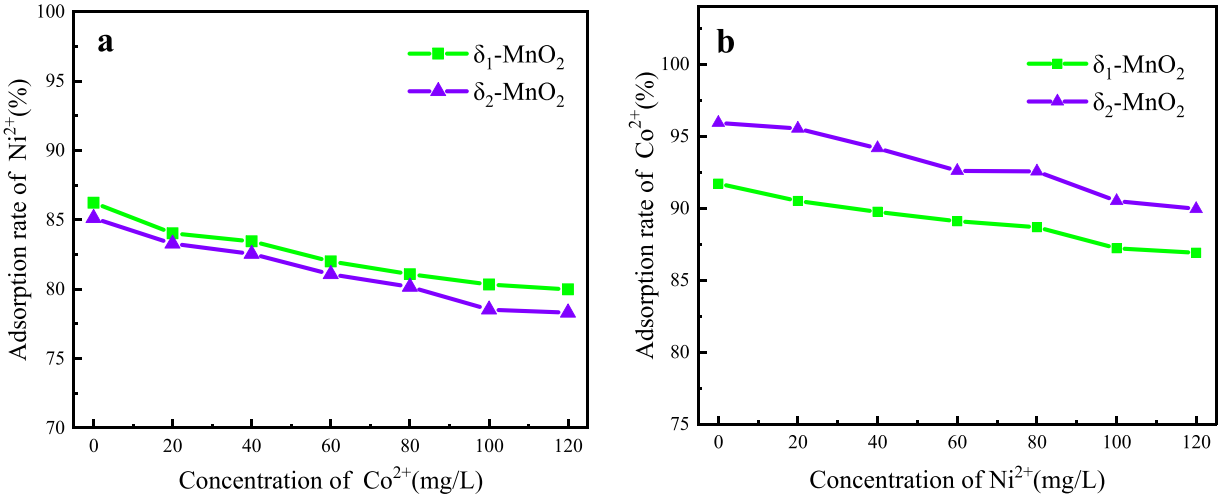

Figure 6. Interaction of cobalt and nickel ions. (a) Effect of Co^{2+} concentration on Ni^{2+} adsorption. (b) Effect of Ni^{2+} concentration on Co^{2+} adsorption.

controlled at 1, 2, 3, 4, 5, 6, 7 and 8, respectively, the adsorption rate of Co^{2+} and Ni^{2+} in manganese sulfate solution by δ-MnO_2 was as shown in Figure 5.

It is obvious from Figure 5 that the adsorption rate of δ-MnO_2 for Co^{2+} and Ni^{2+} increased with the increase of pH value of the manganese sulfate solution. The change trend of the adsorption rate of the two kinds of δ-MnO_2 was similar. When the solution pH increased from 1 to 5, the adsorption rate of the two ions increased slowly, mainly because the concentration of H^+ was high at low pH, and the surface hydroxyl was more likely to react with H^+ to form $\equiv SOH_2^+$. At the same time, the solution pH was less than the isoelectric point and the surface of δ-MnO_2 was positively charged, so the adsorption of Co^{2+} and Ni^{2+} was mainly affected by the structural defects and voids of δ-MnO_2. However, when pH increased from 5 to 8, the adsorption rate increased rapidly. When pH reached 8, the adsorption rates of Co^{2+} and Ni^{2+} by δ-MnO_2 reached the highest. This was because the pH of the solution was obviously higher than the isoelectric point, the negative charge on the surface of MnO_2 increased, the hydroxyl was deprotonated to form $\equiv SO^-$, and then it reacted with Co^{2+} and Ni^{2+} in the solution, so it was easier to adsorb Co^{2+} and Ni^{2+} in the solution. At the same time, when pH = 8, Mn^{2+} in manganese sulfate would be partially consumed and converted to $Mn(OH)_2$. So the appropriate pH value was 7.

2.1.4. Effect of Co^{2+} and Ni^{2+} Concentration. When reaction time was 60 min; reaction temperature was 80 °C; pH value was controlled at 7; the concentration of Ni^{2+} was 100 mg/L; and the concentration of Co^{2+} was 0, 20, 40, 60, 80, 100, and 120 mg/L, respectively, the effect of Co^{2+} concentration on the adsorption of Ni^{2+} in the manganese sulfate solution by δ-MnO_2 was as shown in Figure 6a. When the other conditions were the same; the concentration of Co^{2+} was 100 mg/L; and the concentration of Ni^{2+} was 0, 20, 40, 60, 80, 100, and 120 mg/L, respectively, the effect of Ni^{2+} concentration on the adsorption of Co^{2+} in the manganese sulfate solution by δ-MnO_2 was as shown in Figure 6b.

Figure 6 shows that there is an obvious competitive relationship between Co^{2+} and Ni^{2+} in the adsorption process. The adsorption rate of Ni^{2+} decreases gradually with the increase of Co^{2+} concentration, and the adsorption rate of Co^{2+} decreases gradually with the increase of Ni^{2+} concentration. Co^{2+} is stronger in the adsorption competition. The affinity of hydroxyl to Co^{2+} is relatively large, and there is a difference in the adsorption capacities of two δ-MnO_2 to two ions. δ_1-MnO_2 is more inclined to adsorb Ni^{2+}, and δ_2-MnO_2 is more inclined to

https://doi.org/10.1021/acsomega.2c04240
ACS Omega 2022, 7, 37452−37464

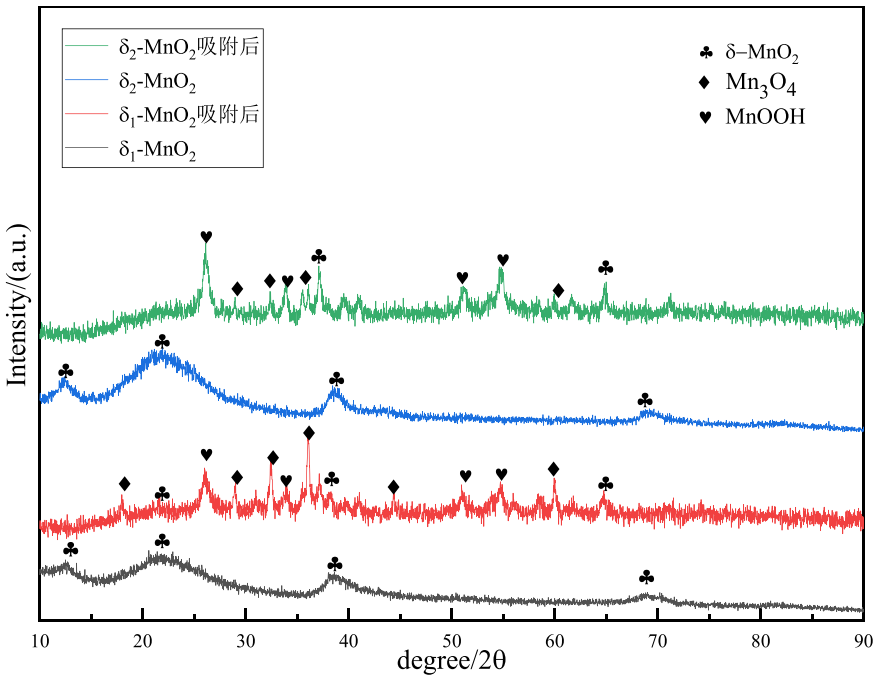

Figure 7. XRD patterns of δ-MnO_2 before and after adsorption.

adsorb Co^{2+}. The affinity and adsorption capacity of manganese dioxide for different metal ions are different. The adsorption order is generally $Pb^{2+} > Cu^{2+} > Co^{2+} > Ni^{2+} > Zn^{2+} > Mn^{2+} > Ca^{2+} > Mg^{2+} > Na^{+}$, which is basically consistent with the order of ionic hydrolysis constants.[53] This is also the reason why Co^{2+} is preferentially adsorbed and Co^{2+} and Ni^{2+} could be adsorbed in the manganese sulfate solution. Considering the adsorption efficiency and adsorption competition, Co^{2+} and Ni^{2+} were set at 80 g/L.

2.2. Study on the Adsorption Mechanism of MnO_2. The optimal adsorption conditions were obtained through the above adsorption experiments, and they were as follows: the Co^{2+} concentration was 80 mg/L, Ni^{2+} concentration was 80 mg/L, reaction time was 60 min, reaction temperature was 80 °C, and pH value was 7. On this basis, products before and after adsorption were characterized by XRD, SEM, EDS surface scanning, IR, and XPS, and the adsorption mechanism of δ-MnO_2 was analyzed in depth.

2.2.1. Phase. The XRD analysis of manganese dioxide before and after Co and Ni adsorption is shown in Figure 7.

According to the XRD pattern analysis, Mn_3O_4 and MnOOH both appear in manganese dioxide after adsorption under the above conditions. This is because the adsorption process is affected by acid points of MnO_2, and the pH could be stabilized only by repeatedly adjusting the pH. In this process, a small amount of Mn^{2+} in the $MnSO_4$ solution became $Mn(OH)_2$ at pH = 7. $Mn(OH)_2$ was oxidized by oxygen to MnOOH in the air, and some MnOOH was further oxidized to Mn_3O_4. These two substances were filtered out together in the adsorbed product, so they appeared in the phase.

2.2.2. Microstructure and Surface Elements. The SEM images of manganese dioxide before and after Co and Ni adsorption are shown in Figure 8.

As shown in Figure 8, δ_1-MnO_2 before adsorption is stacked by nanoparticles with a diameter of 150 nm, forming a cluster of layered structures with large voids. The morphology after adsorption is shown in Figure 8c, which changes from the large

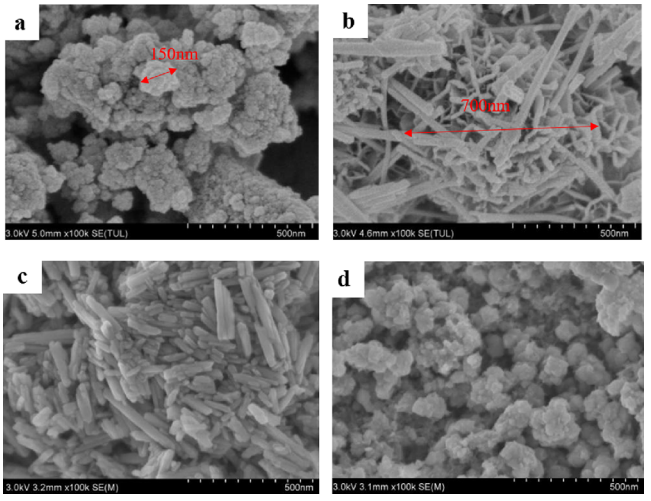

Figure 8. SEM images before and after adsorption: (a) δ_1-MnO_2 before adsorption, (b) δ_2-MnO_2 before adsorption, (c) δ_1-MnO_2 after adsorption, and (d) δ_2-MnO_2 after adsorption.

pore structure of nanoparticles before adsorption to the dense structure of nanorods with different lengths. The δ_2-MnO_2 before adsorption is aggregated by nanorods and has a rich pore structure with a diameter of 700 nm. δ_2-MnO_2 after adsorption transforms into a compact accumulation structure. The large difference in morphology depends on several reasons. First, the surface hydroxyl of MnO_2 combines with a large number of Mn^{2+}, Co^{2+}, and Ni^{2+} in the solution to form a new morphology structure. Second, it could be known that Mn_3O_4 and MnOOH produced in the adsorption process also affected the microstructure of MnO_2. Finally, the porous structure of MnO_2 is occupied by metal ions after adsorption to form a relatively dense structure.

EDS diagrams of two kinds of δ-MnO_2 before adsorption are shown in Figures 9 and 10. The higher the O/Mn ratio of MnO_2 is, the richer the surface oxygen is, and the oxygen coordination

https://doi.org/10.1021/acsomega.2c04240
ACS Omega 2022, 7, 37452−37464

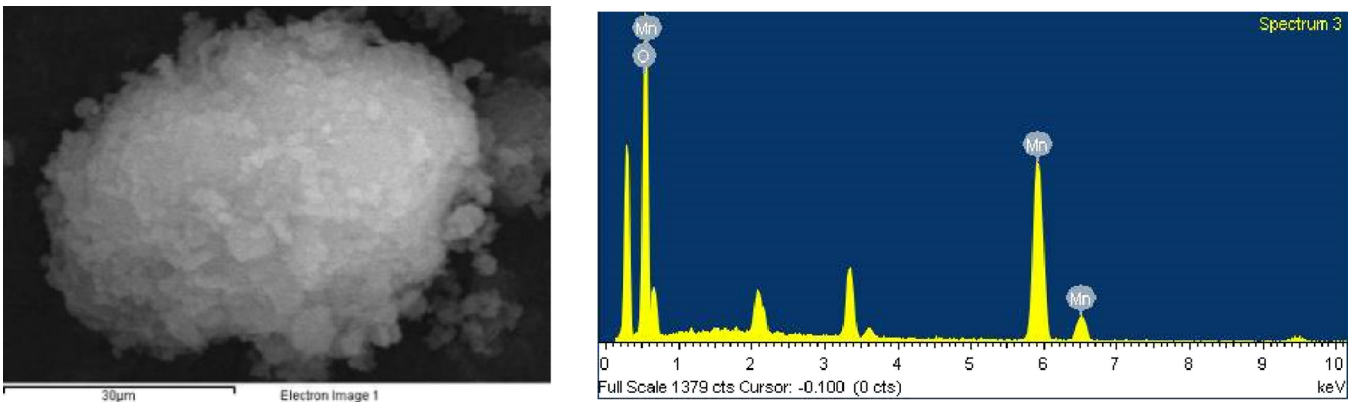

Figure 9. EDS point scan diagram of δ_1-MnO_2.

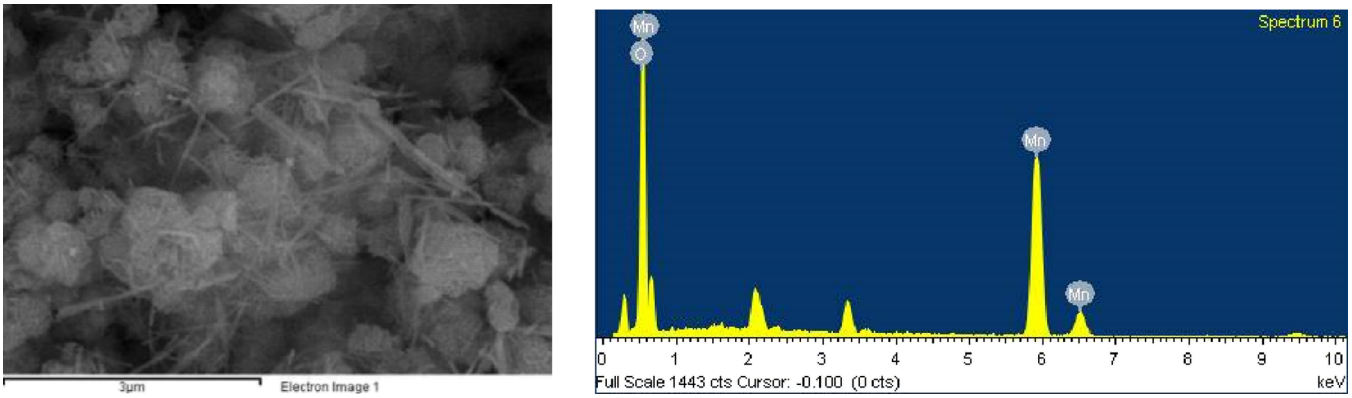

Figure 10. EDS point scan diagram of δ_2-MnO_2.

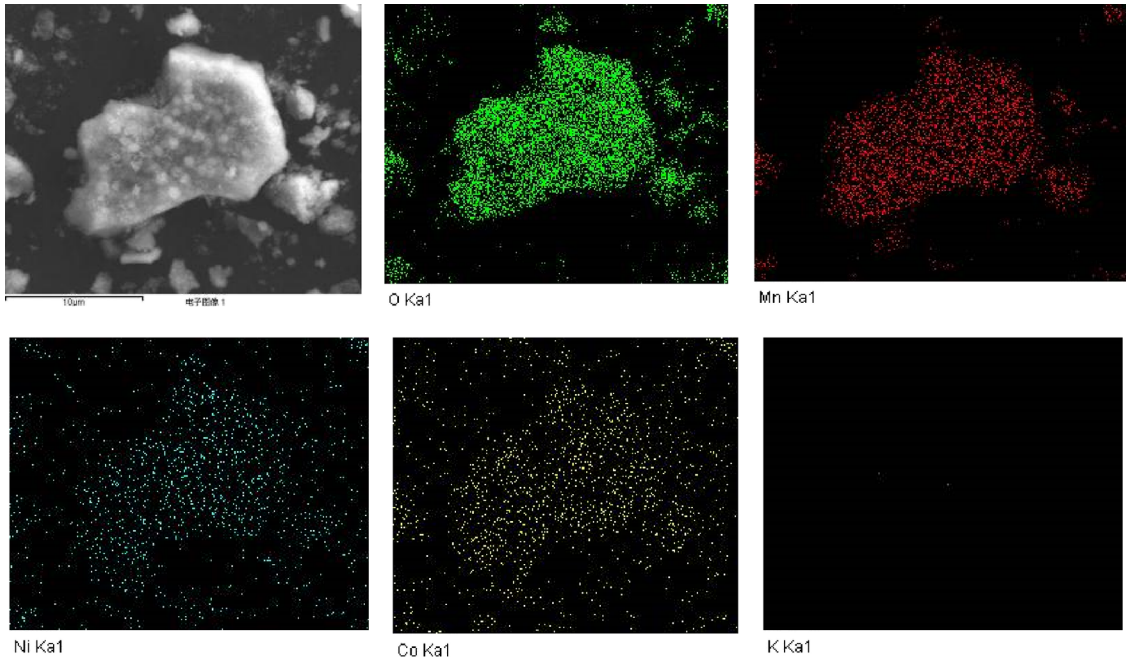

Figure 11. EDS surface scan diagram of δ_1-MnO_2 after adsorption.

around the manganese vacancy is unsaturated, resulting in the formation of a large number of hydroxyl groups on the surface of MnO_2, which is more conducive to the surface complexation reaction. The O/Mn ratios of δ_1-MnO_2 and δ_2-MnO_2 are 2.76 and 2.65, respectively, which indicate that the two kinds of δ-MnO_2 have a high surface oxygen content and could form more hydroxyl functional groups on their surfaces, so they have the potential to become adsorbents with a high adsorption capacity.

It can be seen from Figure 11 that Mn and O in the products adsorbed by δ_1-MnO_2 are still the main two elements, and a large

https://doi.org/10.1021/acsomega.2c04240
ACS Omega 2022, 7, 37452−37464

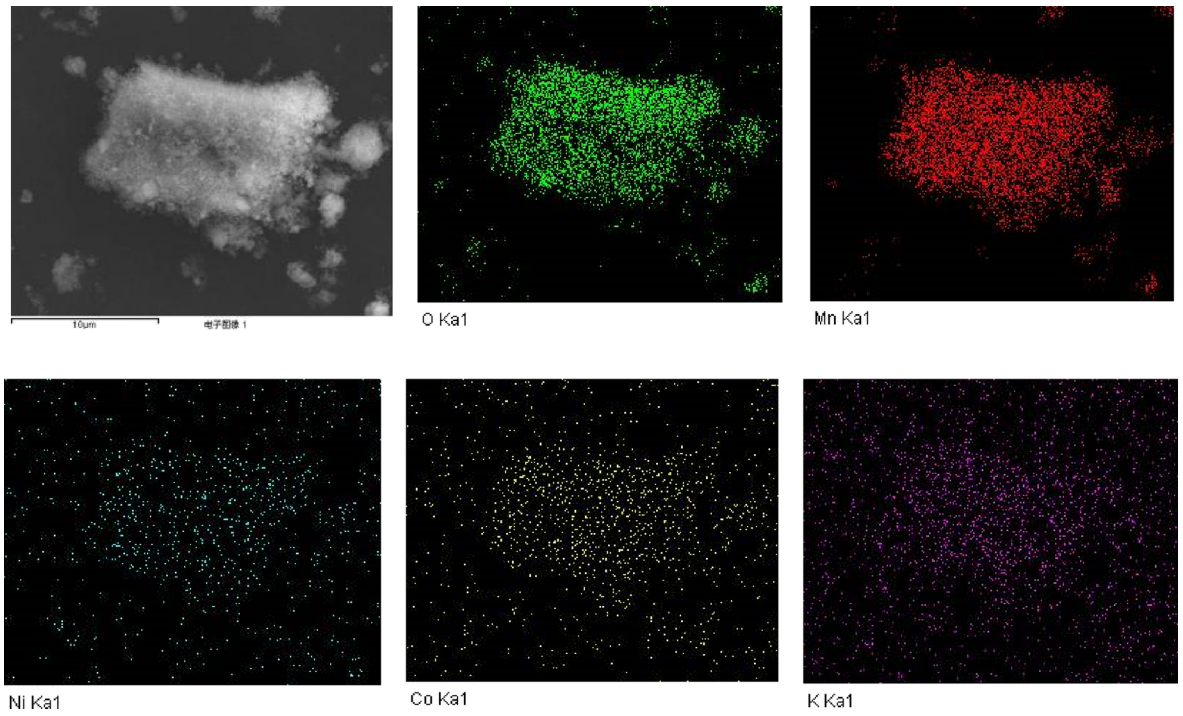

Figure 12. EDS surface scan diagram of δ_2-MnO_2 after adsorption.

number of Co^{2+} and Ni^{2+} are distributed, indicating that Co^{2+} and Ni^{2+} are adsorbed by MnO_2. At the same time, it can be seen that there is still O element distribution in the area without Mn element. This part of oxygen may come from the crystal water formed by MnO_2 adsorbed water. According to the distribution of Co^{2+} and Ni^{2+} elements, it is speculated that it may also come from the oxides of Co and Ni. It can be seen from Table 1 that the O/Mn ratio of δ_1-MnO_2 increased from 2.76 to 3.11 after adsorption. In the process of surface hydroxyl binding to metal ions, with the progress of complexation reaction, O element was increasing. According to $\equiv SO^- + M^{2+} + H_2O \equiv SOMnOH + H^+$, surface hydroxyl ≡SOH reacted with metal ions M to form ≡SOMOH. The second sources of oxygen are crystal water produced during adsorption and manganese oxide in the solution. Co^{2+} and Ni^{2+} ions are mainly distributed on the surface of MnO_2 particles, and a small amount of them is evenly distributed in the gap of MnO_2 particles. It further shows that the hydroxyl complexation reaction on the surface of MnO_2 plays a leading role in the adsorption of Co^{2+} and Ni^{2+}, and MnO_2 pores play an auxiliary role. At the same time, the proportion of the Co element is slightly higher than that of the Ni element. The K ions in the adsorbed δ_1-MnO_2 almost do not exist, and the layered structure of δ-MnO_2 is mainly supported by K ions. The behavior of other metal ions replacing K ions is bound to affect the structure of δ-MnO_2 in the adsorption process.

Figure 12 shows that the distribution of each element in the adsorption products of δ_2-MnO_2 and δ_1-MnO_2 is basically consistent. The only difference is that there is a K element in the adsorption products of δ_2-MnO_2, indicating that the stability of the δ_2-MnO_2 layered structure is stronger. According to Table 2, the O/Mn ratio of δ_2-MnO_2 increased from 2.65 to 2.90. And the element proportion of Co^{2+} and Ni^{2+} shows that the adsorption capacity of δ_2-MnO_2 for Co^{2+} is slightly higher than that of δ_1-MnO_2 and that the adsorption capacity of δ_1-MnO_2 for Ni^{2+} is slightly higher than that of δ_2-MnO_2.

Table 2. The Proportion of Each Element after the Adsorption of Two Kinds of δ-MnO_2

δ-MnO_2	element	Mn	O	Ni	Co	K
δ1-MnO_2	percentage by weight	50.33	45.63	1.87	2.17	0
	atomic percent ratio	23.87	74.34	0.83	0.96	0
δ2-MnO_2	percentage by weight	51.66	43.67	1.67	2.40	0.59
	atomic percent ratio	25.05	72.71	0.76	1.09	0.40

2.2.3. Surface Hydroxyl and Other Groups. The infrared spectral characteristics of manganese dioxide before and after Co and Ni adsorption are shown in Figure 13.

In the δ_1-MnO_2 and δ_2-MnO_2 before adsorption, there are a surface hydroxyl stretching vibration peak near 3400 cm^{-1}, surface hydroxyl bending vibration peak near 1600 and 1100 cm^{-1}, and Mn−O lattice vibration peak near 500−600 cm^{-1}. In addition, there are acetate ion C−O and C−H vibration peaks near 1400 cm^{-1} in δ_1-MnO_2 prepared by manganese acetate. δ_1-MnO_2 and δ_2-MnO_2 have broad and strong hydroxyl vibration peaks, So they are rich in surface hydroxyl, which is more conducive to surface complexation reaction with heavy metal ions so as to achieve an excellent adsorption effect.

In the δ_1-MnO_2 and δ_2-MnO_2 after adsorption, the surface hydroxyl vibration peaks near 3400 and 1600 cm^{-1} are obviously weakened, indicating that a large number of hydroxyls are bound to metal ions, and the utilization rate of hydroxyls is greatly increased. There are new vibration peaks that appeared near 2600 and 2000 cm^{-1}, which are likely to be ≡SOCoOH and ≡SONiOH formed by the complexation of Co^{2+}, Ni^{2+}, and hydroxyl groups on the surface of δ-MnO_2. The enhancement of the vibration peak near 1000 cm^{-1} is caused by the increase of adsorbed water on the surface of δ-MnO_2, which is basically consistent with the EDS surface oxygen scanning analysis. The

https://doi.org/10.1021/acsomega.2c04240
ACS Omega 2022, 7, 37452−37464

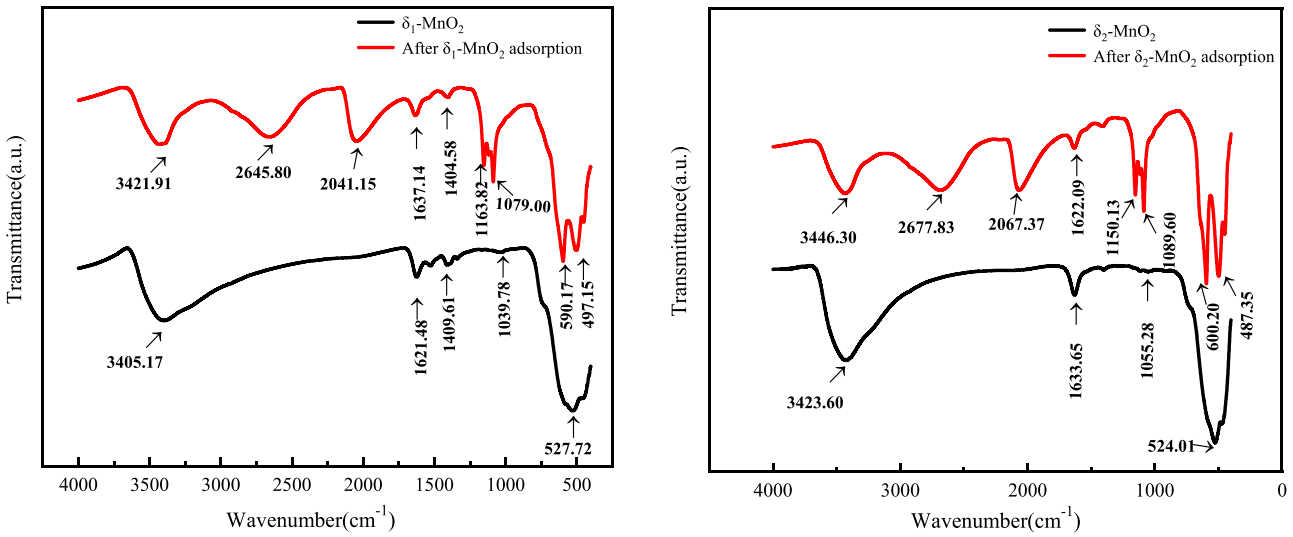

Figure 13. FT-IR spectra of δ-MnO_2 before and after adsorption.

vibration peaks of the Mn-O lattice near 500−600 cm^{-1} moved and were enhanced, which are caused by Mn^{2+} adsorption on the δ-MnO_2 surface or Mn_3O_4 and MnOOH generated from Mn^{2+}.

2.2.4. Atomic Valence State. The XPS spectra of manganese dioxide before and after Co and Ni adsorption are shown in Figure 14.

From Figure 14a, it could be found that the K^+ peak basically disappeared in δ_1-MnO_2 and δ_2-MnO_2 after adsorption. It indicates that interlayer K^+ was replaced by metal cations in the solution. Figure 14b shows that the structure oxygen of δ-MnO_2 has no obvious change after adsorption, but the proportion of adsorbed oxygen increases greatly. This indicates that in the adsorption process of surface hydroxyl, the surface hydroxyl reacts with metal ions (M) to form ≡SOMOH. The oxygen in ≡SOMOH causes the increase of adsorbed oxygen on the surface of δ-MnO_2. Therefore, the adsorbed oxygen content increases with the adsorption. It could be seen from Figure 14c that the peak bond energy of Mn2p decreased after adsorption, indicating that the proportion of low-valent Mn increased, which was related to Mn^{2+} adsorbed by MnO_2 and the Mn_3O_4 and MnOOH generated during the adsorption process. Figure 14d,e could also verify that Co^{2+} and Ni^{2+} were adsorbed by MnO_2, but the adsorption amounts of Co^{2+} and Ni^{2+} were relatively small compared with the adsorbent body, so the 2p peak was not obvious. It could be speculated that the combined valence of Co and Ni was bivalent according to the binding energy.

2.2.5. Adsorption Mechanism. According to the above research, the mechanism of manganese dioxide adsorbing Co and Ni ions is as follows. The protonation and deprotonation of surface hydroxyl (≡SOH) occurred first when MnO_2 was in contact with solution.[53,55] The reaction formulas are shown in formula 1 and formula 2.

$$\equiv SOH + H^+ \leftrightarrows \equiv SOH^{2+} \quad (1)$$

$$\equiv SOH(+OH^-) \leftrightarrows \equiv SO^- + H^+(+H_2O) \quad (2)$$

The hydroxyl group underwent deprotonation reaction to form $\equiv SO^-$ and then complexed with Co^{2+} and Ni^{2+} in the solution. The reaction formulas are shown in formula 4 and formula 5.

$$\equiv SOH + Co^{2+} \leftrightarrows \equiv SOCo^+ + H^+ \quad (3)$$

$$\equiv SOH + Ni^{2+} \leftrightarrows \equiv SONi^+ + H^+ \quad (4)$$

Due to the difference in the complexing ability of hydroxyl groups on the surface of MnO_2 to different cations, there would be an ion exchange reaction on the surface of δ-MnO_2. For example, the K^+ supporting the layered structure was replaced by metal ions, and a large number of Mn^{2+}, Co^{2+}, and Ni^{2+} entered the macropore structure of MnO_2, resulting in the change of its microstructure. The complex reaction produced $\equiv SOCo^+$ and $SONi^+$, so Co and Ni appeared on the surface element distribution of δ-MnO_2 after adsorption. A large number of surface hydroxyl groups of MnO_2 combined with metal ions, and the utilization rate of hydroxyl groups increased, resulting in the weakening of hydroxyl vibration peak. The surface hydroxyl group reacted with metal ions (M) to form ≡SOMOH. The oxygen in ≡SOMOH still only existed on the surface of MnO_2 in the form of adsorbed oxygen. Therefore, the adsorbed oxygen content increased with the adsorption. After the complexation reaction, Co^{2+} and Ni^{2+} appeared on the surface of MnO_2, Mn^{2+} was also adsorbed by MnO_2, and Mn_3O_4 and MnOOH were produced during the adsorption process, which would increase the proportion of low-valence Mn.

3. EXPERIMENTS

3.1. Experimental Materials and Equipment. Sulfuric acid, ammonia, potassium permanganate, manganese acetate, manganese sulfate monohydrate, nickel sulfate hexahydrate, and cobalt sulfate heptahydrate used in the experiment were all analytically pure reagents and produced by Tianjin Comitry Co., Ltd.

The experimental equipment used was as follows: the PHS-25 digital pH meter was produced by Shanghai Yidian Scientific Instruments Co., Ltd.; the HH-3 constant-temperature water bath boiler was produced by Shanghai Scientific Analysis Experimental Instruments Co., Ltd.; the DHG-905A constant-temperature drying box was produced by Beijing Yongguangming Medical Instruments Co., Ltd.; the P4Z vacuum pump was produced by Beijing Jinghui Kaiye Co., Ltd.; the PL2002 electronic analysis balance was produced by Mettler-Toledo Instruments (Shanghai) Co., Ltd.; the JJ-1 precision booster electric stirrer was produced by Changzhou Aohua Instruments Co., Ltd.; the SHA-C constant-temperature water bath shaker

https://doi.org/10.1021/acsomega.2c04240
ACS Omega 2022, 7, 37452−37464

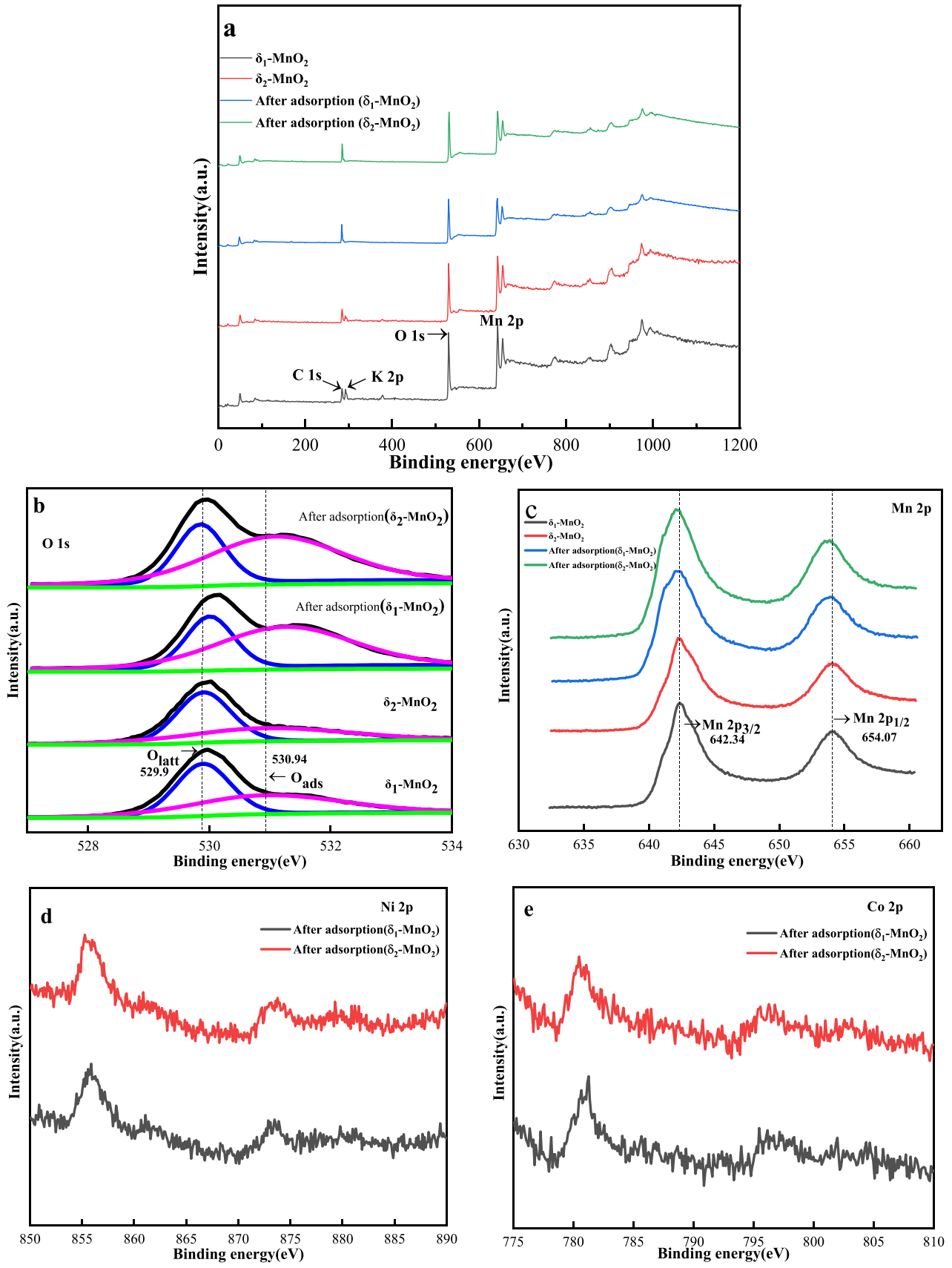

Figure 14. XPS spectra of δ-MnO_2 before and after adsorption: (a) full spectrum, (b) O1s spectrum, (c) Mn2p spectrum, (d) Ni2p spectrum, and (e) Co2p spectrum.

https://doi.org/10.1021/acsomega.2c04240
ACS Omega 2022, 7, 37452−37464

reciprocating oscillator was produced by Changzhou Guohua Electric Co., Ltd.; the SX-4-10 box resistance furnace was produced by Tianjin Tate Scientific Instruments Co., Ltd.; the HY-5B rotary oscillator was produced by Changzhou Langyue Instruments Manufacturing Co., Ltd.; and the A3AFG-13 flame atomic absorption spectrometer was produced by Beijing Pusan General Instrument Co., Ltd.

3.2. Experimental Process. The synthesis steps of δ_1-MnO_2 are as follows: 0.1 mol/L potassium permanganate solution 300 mL and 0.15 mol/L manganese acetate solution 150 mL were prepared with deionized water, respectively. The potassium permanganate solution was first stirred by magnetic force for 30 min, and then the prepared concentration of manganese acetate solution was added. The stirring reaction was carried out at 80 °C for 6 h. After the solution was cooled to room temperature, the black precipitate was obtained. The product was washed with deionized water many times, and the impurity ions were removed. The product was dried at 100 °C for 5 h.

The steps of synthesizing δ_2-MnO_2 are as follows: 0.1 mol/L potassium permanganate solution 300 mL and 0.15 mol/L manganese sulfate solution 150 mL were prepared with deionized water, respectively. The potassium permanganate solution was first stirred by magnetic force for 30 min, and then the prepared concentration of $MnSO_4$ solution was added. The magnetic stirring reaction was carried out at 80 °C for 6 h. After the solution was cooled to room temperature, the brown and black precipitate was obtained. The product was washed with deionized water many times, and the impurity ions were removed. The product was dried at 100 °C for 5 h.

A mixed solution of Mn^{2+}, Ni^{2+}, and Co^{2+} was prepared with manganese sulfate monohydrate, nickel sulfate hexahydrate, cobalt sulfate heptahydrate, and deionized water. The pH of the solution was adjusted with 10% ammonia, and a certain amount of prepared δ-MnO_2 was added. The solution was continuously stirred in a constant-temperature water bath at a certain temperature. Due to the influence of the pH of MnO_2 equi-acidity point, the pH of the solution would decrease to a certain value. The pH of the solution was adjusted to 7 by dropping ammonia. With the progress of the reaction, the pH of the solution decreased again and continued to be adjusted until the pH did not decrease. The adsorption experiments were carried out by controlling the reaction time, reaction temperature, reaction pH, MnO_2 addition, Mn^{2+} concentration, Co^{2+} concentration, and Ni^{2+} concentration. After the adsorption, the solution was quickly filtered. The concentrations of Ni^{2+} and Co^{2+} in the filtrate were determined by an A3AFG-13 flame atomic absorption spectrometer, and the filter residue was further characterized and analyzed after drying.

3.3. Characterization Methods. The adsorption rate formula is shown in formula 5:

$$Q = \frac{c_0 - c}{c_0} \times 100\% \quad (5)$$

c_0 is the initial concentration of impurity ions before adsorption, and c is the concentration of impurity ions after adsorption.

In the experiment, the phase identification was done by a Bruker D8 ADVANCE diffraction analyzer from Bruker, Germany. The microstructure and energy spectrum were analyzed by an SU8020 scanning electron microscope from Hitachi, Japan. The FT-IR analysis was collected on a Nicolet iS10 infrared spectrometer produced by Nigaoli, USA. The XPS data were collected on a Thermo ESCALAB 250Xi electronic energy spectrometer produced by ThermoFisher Scientific, USA.

4. CONCLUSIONS

Two kinds of δ-MnO_2 were prepared under controlled conditions. With δ-MnO_2 addition amount of 10 g/L, Co^{2+} and Ni^{2+} in the manganese sulfate solution with Mn^{2+} concentration of 20 g/L were adsorbed and removed, and better adsorption conditions were obtained. They were as follows: When Co^{2+} concentration was 80 mg/L, Ni^{2+} concentration was 80 mg/L, reaction time was 60 min, reaction temperature was 80 °C, and pH value was 7, the adsorption rate of Co^{2+} and Ni^{2+} by the two kinds of δ-MnO_2 reached more than 80%. The phase, microstructure, surface hydroxyl, surface element content, and surface oxygen of the δ-MnO_2 were analyzed after adsorption. MnOOH phase was found in both kinds of δ-MnO_2 after adsorption. δ_1-MnO_2 and δ_2-MnO_2 showed dense rod-like structures with different lengths and flake-like structures of fine particles. Co and Ni were distributed on the surface and gap of MnO_2 particles after adsorption, the atomic percentage of Co was slightly higher than that of Ni, and the oxygen content would increase after adsorption. After adsorption, the surface hydroxyl vibration peaks of δ-MnO_2 decreased, and new vibration peaks appeared near 2668.32, 1401.00, and 2052.19 cm^{-1}, indicating that cations such as Co^{2+} and Ni^{2+} complexed with hydroxyl and new vibration peaks were formed on the surface of δ-MnO_2. After adsorption, partial Co^{2+} and Ni^{2+} appeared on the surface of δ-MnO_2, and the surface oxygen increased. The adsorption mechanism of manganese dioxide is revealed, as follows: δ-MnO_2 reacted with metal ions (M) to form ≡SOMOH through surface hydroxyl groups so as to realize the adsorption and removal of Co^{2+} and Ni^{2+} in the manganese sulfate solution.

AUTHOR INFORMATION

Corresponding Author

Haifeng Wang − *School of Materials and Metallurgy, Guizhou University, Guiyang 550025, China; Research Center for Engineering Technology of Manganese Materials for Battery, Tongren 554300, China; Guizhou Provincial Key Laboratory of Metallurgical Engineering and Process Energy Conservation, Guiyang 550025, China*; Email: 380889450@qq.com

Authors

Pan Yang − *School of Materials and Metallurgy, Guizhou University, Guiyang 550025, China; Guizhou Provincial Key Laboratory of Metallurgical Engineering and Process Energy Conservation, Guiyang 550025, China*

Jiawei Wang − *School of Materials and Metallurgy, Guizhou University, Guiyang 550025, China; Research Center for Engineering Technology of Manganese Materials for Battery, Tongren 554300, China; Guizhou Provincial Key Laboratory of Metallurgical Engineering and Process Energy Conservation, Guiyang 550025, China*

Song Wang − *School of Materials and Metallurgy, Guizhou University, Guiyang 550025, China; Guizhou Provincial Key Laboratory of Metallurgical Engineering and Process Energy Conservation, Guiyang 550025, China*

Chunyuan Yang − *School of Materials and Metallurgy, Guizhou University, Guiyang 550025, China; Guizhou Provincial Key Laboratory of Metallurgical Engineering and Process Energy Conservation, Guiyang 550025, China*

https://doi.org/10.1021/acsomega.2c04240
ACS Omega 2022, 7, 37452−37464

Pingyuan Zhao − *School of Materials and Metallurgy, Guizhou University, Guiyang 550025, China; Guizhou Provincial Key Laboratory of Metallurgical Engineering and Process Energy Conservation, Guiyang 550025, China*

Bifang Huang − *School of Materials and Metallurgy, Guizhou University, Guiyang 550025, China; Guizhou Provincial Key Laboratory of Metallurgical Engineering and Process Energy Conservation, Guiyang 550025, China*

Qin Wang − *School of Materials and Metallurgy, Guizhou University, Guiyang 550025, China; Guizhou Provincial Key Laboratory of Metallurgical Engineering and Process Energy Conservation, Guiyang 550025, China*

Complete contact information is available at: https://pubs.acs.org/10.1021/acsomega.2c04240

Author Contributions

#P.Y. and J.W.W. contributed equally to this work

Notes

The authors declare no competing financial interest.

■ ACKNOWLEDGMENTS

The funding supports for this study were obtained from the National Natural Science Foundation of China (51864012), Guizhou Provincial Science Cooperation Program ([2016] 5302, [2017] 5788, [2018] 5781, [2019] 1411, [2019] 2841, [2022] 020, and [2022] 003), and Major special projects in Tongren City, Guizhou Province (2021) 13. The authors sincerely thank the reviewers for their views and suggestions to further improve the quality of the manuscript.

■ REFERENCES

(1) Liu, Y.; Ming, X. Q.; Huang, B. H.; Liu, H. H.; Yuan, M. L. Control of Fluorine Content in High Purity Manganese Sulfate Prepared By Fluorination. *Min. Metall. Eng.* **2021**, *41*, 98−102.

(2) He, Y. H.; Zhang, H. J.; Xiong, S. $MnSO_4$ solution and preparation of battery grade high purity manganese sulfate. *Hydrometallurgy* **2019**, *38*, 380−384.

(3) Zhao, Y. H.; Wu, R. L.; Hu, P. Study on impurity characteristics and purification process of high purity manganese sulfate. *World Nonferrous Metals* **2020**, *1*, 186−188.

(4) Chen, Z. H.; Feng, H. C.; Luo, Y. Y.; Lei, J.; Huang, X. Determination of silicon content in manganese sulfate for battery and battery materials. *Shanxi Chemical Industry* **2021**, *41*, 35−36.

(5) He, B. H. Experimental study on removal of heavy metals from industrial manganese sulfate. *China Manganese Industry* **2021**, *39*, 56−60.

(6) Wang, Y.; Huang, P.; Li, C. Flexible and self-supported manganese dioxide/S composite cathode for high electrochemical performance. *Ionics* **2021**, *27*, 5037−5042.

(7) Parveen, N.; Ansari, S. A.; Al-Arjan, W. S.; Ansari, M. O. Manganese dioxide coupled with hollow carbon nanofiber toward high-performance electrochemical supercapacitive electrode materials. *J. Sci.: Adv. Mater. Devices* **2021**, *6*, 472−482.

(8) Mahdi, F.; Javanbakht, M.; Shahrokhian, S. Anodic pulse electrodeposition of mesoporous manganese dioxide nanostructures for high performance supercapacitors. *J. Alloys Compd.* **2021**, *887*, 161376.

(9) Ahmed, S.; Ahmad, Z.; Kumar, A.; Rafiq, M.; Vashistha, V. K.; Ashiq, M. N.; Kumar, A. Effective removal of methylene blue using nanoscale manganese oxide rods and sphere derived from different precursors of manganese. *J. Phys. Chem. Solids* **2021**, *155*, 110121.

(10) Fu, D. J.; Wang, H. F.; Gou, B. B.; Li, M. D.; Wang, J. W. Preparation of Octahedral Mn_3O_4 by Liquid Phase Method. *J. Phys.: Conf. Ser.* **2022**, *2166*, No. 012067.

(11) Zhang, H.; Song, D.; Zhang, Q.; Huang, X. P. Evaporation-Cooling Coupling Method to Remove the Calcium and Magnesium Impurities in Leaching Solution of Manganese Ore. *IOP Conference Series: Earth and Environmental Science* **2021**, *651*, No. 042055.

(12) Wang, Y. J.; Wang, W. N.; Liu, Y. L.; Liu, F.; Chen, X. Y. Removal of Heavy Metals from Manganese Sulfate Solution and Preparation Battery-level Manganese Sulfate. *Nonferrous Metals (Extractive Metallurgy)* **2020**, *11*, 79−84.

(13) Tian, J. Y.; Wang, H. F.; Kuang, S. D.; Yang, Q. K.; Hu, P.; Wang, J. W. Study on Removal of Heavy Metals from Manganese Sulfate Solution by Sulfide. *Nonferrous Metals (Extractive Metallurgy)* **2019**, *12*, 6−10.

(14) Lin, D. Z. Experimental Study on Purification of Cadmium from Manganese Sulfate Solution by Manganese Sulfide. *China Steel Focus* **2020**, *11*, 39−40.

(15) Lin, Q. Q.; Gu, G. H.; Wang, H. Separation of Manganese from calcium and magnesium in sulfate solutions via carbonate precipitation. *Trans. Nonferrous Met. Soc. China* **2016**, *26*, 1118−1125.

(16) Yan, S.; Qiu, Y. R. Preparation of electronic grade Manganese sulfate from leaching solution of ferromanganese slag. *Trans. Nonferrous Met. Soc. China* **2014**, *24*, 3716−3721.

(17) He, G. X.; He, L. H.; Zhao, Z. W. Thermodynamic study on phosphorus removal from tungstate solution via magnesium salt precipitation method. *Trans. Nonferrous Met. Soc. China* **2013**, *23*, 3440−3447.

(18) Chen, X. L.; Wang, H. F.; Wang, J. W.; Zhao, P. Y. Removal of Cobalt and Nickel from Manganese Sulfate Leachate by Carbonization. *Conservation and Utilization of Mineral Resources* **2020**, *40*, 103−107.

(19) Chen, X. L.; Wang, H. F.; Wang, J. W. Removal of Calcium and Magnesium from Manganese Sulfate Leaching Solution via a Reverse Precipitation by Carbonation. *Kuangye Gongcheng (Changsha, China)* **2020**, *40*, 82−85+93.

(20) Jantunen, N.; Kauppinen, T.; Salminen, J.; Virolainen, S.; Lassi, U.; Sainio, T. Separation of zinc and iron from secondary manganese sulfate leachate by solvent extraction. *Miner. Eng.* **2021**, *173*, 107200.

(21) Chen, H. Y.; Wang, K. T.; Ming, X. Q.; Zhan, F.; Muhammad, Y.; Zhan, Y. Z.; Wei, W. J.; Li, H. Q. The Efficient Removal of Calcium and Magnesium Ions from Industrial Manganese Sulfate Solution through the Integrated Application of Concentrated Sulfuric Acid and Ethanol. *Metals* **2021**, *11*, 1339.

(22) Wang, H. F.; You, X. Y.; Tian, J. Y.; Chen, X. L.; Wang, J. W. Solubility and crystallinity of manganese, magnesium and ammonium double salt systems. *Mater. Express* **2021**, *11*, 540−550.

(23) Zhang, H. S.; Hu, X.; Li, T. X.; Zhang, Y. X.; Xu, H. X.; Sun, Y. Y.; Gu, X. Y.; Gu, C.; Luo, J.; Gao, B. MIL series of metal organic frameworks (MOFs) as novel adsorbents for heavy metals in water: A review. *J. Hazard. Mater.* **2022**, *429*, 128271.

(24) Zhao, P.; Huang, Z. B.; Ma, Q.; Zhang, B. L.; Wang, P. Artificial humic acid synthesized from food wastes: An efficient and recyclable adsorbent of Pb (II) and Cd (II) from aqueous solution. *Environ. Technol. Innovation* **2022**, *27*, 102399.

(25) Ihsanullah, I. Applications of MOFs as adsorbents in water purification: Progress, challenges and outlook. *Current Opinion in Environmental Science & Health* **2022**, *26*, 100335.

(26) Thakur, A. K.; Singh, R.; Teja, P. R.; Pundir, V. Green adsorbents for the removal of heavy metals from Wastewater: A review. *Mater. Today: Proc.* **2022**, *57*, 1468−1472.

(27) Zaimee, M. Z. A.; Sarjadi, M. S.; Rahman, M. L. Heavy Metals Removal from Water by Efficient Adsorbents. *Water* **2021**, *13*, 2659.

(28) Egorova, A. A.; Bushkova, T. M.; Kolesnik, I. V.; Yapryntsev, A. D.; Kottsov, S. Y.; Baranchikov, A. E. Selective Synthesis of Manganese Dioxide Polymorphs by the Hydrothermal Treatment of Aqueous $KMnO_4$ Solutions. *Russ. J. Inorg. Chem.* **2021**, *66*, 146−152.

(29) Ma, J. P.; Zhao, Q. Y.; Wang, C. Removal of heavy metal ions by manganese dioxide-based nanomaterials and mechanism research: A review. *Environ. Chem.* **2020**, *39*, 687−703.

(30) Zou, Z. H.; He, S. F.; Han, C. Y.; Zhang, L. Y.; Luo, Y. M. Progress of Research onTreatment of Heavy Metal Wastewater by Adsorption. *Environ. Prot. Sci.* **2010**, *36*, 22−24.

(31) Meng, K. Y.; Wu, X. W.; Zhang, X. Y.; Su, S. M.; Huang, Z. H.; Min, X.; Liu, Y. G.; Fang, M. H. Efficient Adsorption of the Cd(II) and As(V) Using Novel Adsorbent Ferrihydrite/Manganese Dioxide Composites. *ACS Omega* **2019**, *4*, 18627−18636.
(32) Maneechakr, P.; Mongkollertlop, S. Investigation on adsorption behaviors of heavy metal ions (Cd^{2+}, Cr^{3+}, Hg^{2+} and Pb^{2+}) through low-cost/active manganese dioxide-modified magnetic biochar derived from palm kernel cake residue. *J. Environ. Chem. Eng.* **2020**, *8*, 104467.
(33) Tao, W. Q.; Lv, R. W.; Tao, Q. Q. Facile Preparation of Novel Manganese Dioxide Modified Nanofiber and Its Uranium Adsorption Performance. *J. Appl. Math. Phys.* **2021**, *09*, 1837−1852.
(34) Cheng, M. M.; Yao, C. X.; Su, Y.; Liu, J. L.; Xu, L. J.; Hou, S. F. Synthesis of membrane-type graphene oxide immobilized manganese dioxide adsorbent and its adsorption behavior for lithium ion. *Chemosphere* **2021**, *279*, 130487.
(35) Zhang, H. P.; Xu, F. F.; Xue, J. Y.; Chen, S. Y.; Wang, J. J.; Yang, Y. J. Enhanced removal of heavy metal ions from aqueous solution using manganese dioxide-loaded biochar: Behavior and mechanism. *Sci. Rep.* **2020**, *10*, 6067.
(36) Yang, R. J.; Fan, Y. Y.; Ye, R. Q.; Tang, Y. X.; Cao, X. H.; Yin, Z. Y.; Zeng, Z. Y. MnO_2-Based Materials for Environmental Applications. *Adv. Mater.* **2021**, *33*, 2004862.
(37) Shi, W. H.; Liu, X. Y.; Deng, T. Q.; Huang, S. Z.; Ding, M.; Miao, X. H.; Zhu, C. Z.; Zhu, Y. H.; Liu, W. X.; Wu, F. F.; Gao, C. J.; Yang, S. W.; Yang, H. Y.; Shen, J. N.; Cao, X. H. Enabling Superior Sodium Capture for Efficient Water Desalination by a Tubular Polyaniline Decorated with Prussian Blue Nanocrystals. *Adv. Mater.* **2021**, *32*, 1907404.
(38) Wang, X. H.Study on adsorption effects of different crystalline MnO_2 adsorbents on thallium and antimony in water. *Xi'an Polytechnic University***2018**.
(39) Kong, L. G.; Zhu, Z. L.Adsorption of several heavy metal ions in micro-polluted water by δ-MnO_2. *China Sustainable Development Forum 2006[C]*. 2006. in Chinese
(40) Kanungo, S. B.; Tripathy, S. S.; Mishra, S.; et al. Adsorption of Co^{2+}, Ni^{2+}, Cu^{2+}, and Zn^{2+} onto amorphous hydrous manganese dioxide from simple (1-1) electrolyte solutions. *J. Colloid Interface Sci.* **2004**, *269*, 11−21.
(41) Oscarson, D. W.; Huang, P. M.; et al. Kinetics of oxidation of arsenite by various manganesedioxides. *Soil Sci. Soc. Am. J.* **1983**, *47*, 644−648.
(42) Chen, H.; Ye, Z. J. The study on adsorption of As(III) from wastewater by different types of MnO_2. *China Environ. Sci.* **1998**, *2*, 126−130.
(43) Li, S.*Research on Adsorption Efficiency of Nickle Ion by Synthetic Manganese Oxides*; Chongqing University, 2015. in Chinese
(44) Yao, L.N.*Arsenic Adsorption Performance of Manganese Oxide Nanoparticles*. Qinghai Institute of Salt Lakes, Chinese Academy of Sciences, 2018. in Chinese
(45) Xia, W. T.; Zhao, Z. W.; Ren, Z. D. A Exploratory Researchondeep Removal Trace Molybdenum from Manganese Sulfate Solution with Powder Electrolytic Manganese Dioxide. *China's Manganese Industry* **2008**, *04*, 30−33.
(46) Xia, W. T.; Zhao, Z. W.; Chen, A. L. Research on chemical manganese dioxide adsorbent for removing molybdenum from manganese sulfate solution. *Chin. Battery Ind.* **2008**, *13*, 363−366.
(47) Chen, X. L.; Wang, H. F.; Wang, J. W. Experimental Study on the Removal of Molybdenum from Manganese Sulfate Solution with Electrolytic Manganese Anode Slag. *Metal Mine* **2021**, *05*, 125−129.
(48) Wang, H. F.; Chen, X. L.; Zhao, P. Y.; Gao, Z. W.; You, X. Y.; Tian, J. Y.; Wang, J. W. Preparation of New Nano-MnO_2 and Its Molybdenum Adsorption in Manganese Sulfate Solution. *Nanosci. Nanotechnol. Lett.* **2020**, *12*, 1070−1079.
(49) Xue, W. L.; Yi, H.; Lu, Y. L.; Xia, L.; Meng, D. L.; Song, S. X.; Li, Y. T.; Wu, L.; Farías, M. E. Combined electrosorption and chemisorption of As(III) in aqueous solutions with manganese dioxide as the electrode. *Environ. Technol. Innovation* **2021**, *24*, 101832.
(50) Chen, J. W.; Chen, W.; Huang, M.; Tang, H. Y.; Zhang, J.; Wang, G.; Wang, R. L. Metal organic frameworks derived manganese dioxide catalyst with abundant chemisorbed oxygen and defects for the efficient removal of gaseous formaldehyde at room temperature. *Appl. Surf. Sci.* **2021**, *565*, 150445.
(51) Christian, F. B.; Oliver, S. F.; Jordan, B.; Manuel, B.; Harald, G.; Kai, P. B.; Hans, M.; Henning, D. B. Revealing the Local pH Value Changes of Acidic Aqueous Zinc Ion Batteries with a Manganese Dioxide Electrode during Cycling. *J. Electrochem. Soc.* **2020**, *167*, No. 020545.
(52) Xia, X. The relation between chemical, physical properties and electrochemical activity form anganese dioxides(8). *Battery Bimon.* **2007**, *04*, 271−274.
(53) Li, M. D.; Wang, J. W.; Gou, B. B.; Fu, D. J.; Wang, H. F.; Zhao, P. Y. Relationship between Surface Hydroxyl Complexation and Equi-Acidity Point pH of MnO_2 and Its Adsorption for Co^{2+} and Ni^{2+}.ACS. *Omega* **2022**, *7*, 9602−9613.
(54) Zhang, H.P.*Adsorptive Removal of Lead Ions from Aqueous Solution Using Manganese Oxides Materials*. Nanjing University, 2017, in Chinese.
(55) Hiroki, T.; Tatsuya, O.; Masaichi, N.; Ryusaburo, F. Acid-Base Dissociation of Surface Hydroxyl Groups on Manganese Dioxide in Aqueous Solutions. *J. Electrochem. Soc.* **2019**, *136*, 2782.

https://doi.org/10.1021/acsomega.2c04240
ACS Omega 2022, 7, 37452−37464